Inter J Nav Archit Oc Engng (2012) 4:162~171
http://dx.doi.org/10.2478/IJNAOE-2013-0087

Two-dimensional modeling of stepped planing hulls with open and pressurized air cavities

Konstantin I. Matveev

School of Mechanical and Materials Engineering, Washington State University, Pullman, USA

ABSTRACT: *A method of hydrodynamic discrete sources is applied for two-dimensional modeling of stepped planing surfaces. The water surface deformations, wetted hull lengths, and pressure distribution are calculated at given hull attitude and Froude number. Pressurized air cavities that improve hydrodynamic performance can also be modeled with the current method. Presented results include validation examples, parametric calculations of a single-step hull, effect of trim tabs, and performance of an infinite series of periodic stepped surfaces. It is shown that transverse steps can lead to higher lift-drag ratio, although at reduced lift capability, in comparison with a stepless hull. Performance of a multi-step configuration is sensitive to the wave pattern between hulls, which depends on Froude number and relative hull spacing.*

KEY WORDS: Planing boat; Stepped hull; Air-cavity ship; Method of hydrodynamic singularities.

INTRODUCTION

Planing hulls are commonly used for high-speed water transportation. In the planing mode, hulls skim on the water surface (Fig. 1a), and the dominant supporting force is of hydrodynamic rather than hydrostatic nature. Relatively light or very fast planing boats additionally benefit from using transverse steps on the hull bottom (Fig. 1b). Such steps reduce wetted surface area, improving hydrodynamic performance, and usually decrease operating trim angles, which also leads to better stability properties. That is why many fast pleasure and racing boats, hulls of hydrofoil craft, and wing-in-ground effect vehicles are made with steps in the bottom structure. Novel fast boats with large-area air pockets on the bottom also rely on transverse steps for initiating the drag-reducing air-ventilated cavities (Matveev, 2005). The pressure inside these cavities can exceed the atmospheric pressure, thus generating additional lift (Fig. 1c).

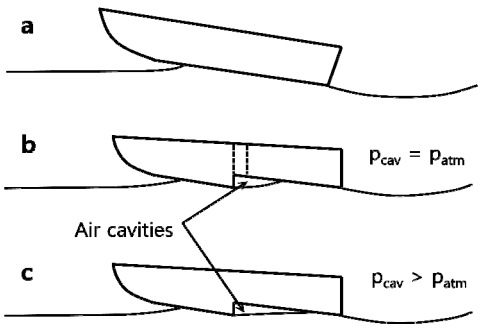

Fig. 1 Planing hulls: (a) stepless hull, (b) stepped hull with open cavity, and (c) stepped hull with pressurized cavity.

Corresponding author: *Konstantin I. Matveev*
e-mail: *matveev@wsu.edu*

Numerous investigations of planing hull hydrodynamics can be found in the literature (e.g., Savitsky, 1964; Payne, 1988; Faltinsen, 2005). However, most studies address stepless hulls. The most common practical approach for such hulls involves added-mass strip theories (e.g., Martin, 1978; Benedict, et al., 2002), although some boundary-element methods (e.g., Doctors, 1974; Lai and Troesch, 1996) and even computationally expensive finite-volume viscous codes (e.g., Caponetto, 2001) have also been applied. For modeling stepped planing configurations, it is necessary to calculate the water surface deformation behind front hulls and account for non-uniform incident flow for rear positioned hulls.

The goal of this paper is to show an application of a method of hydrodynamic singularities, specifically a variant based on discrete sources, for modeling stepped planing surfaces that may include pressurized air cavities. This method has been previously used for hydrodynamic calculations of stepless planing hulls (Matveev and Ockfen, 2009) and air cavities under infinite horizontal solid surfaces (Matveev, 2007). A description of the theoretical model in the next section is followed by validation examples and sample parametric calculations of a single-step two-hull setup and a configuration with multiple steps.

MATHEMATICAL MODEL

A general schematic of a two-dimensional water flow around a stepped hull with small trim angle is shown in Fig. 2a. The flow is assumed to be steady, irrotational, incompressible, and inviscid. The flow is uniform far upstream of the front hull. The flow is sufficiently fast to ensure separation at hull transom edge points. The hull submergences and trim angles are treated as known input parameters. In the case of given weight and center of gravity of the hull and unknown trim and sinkage, one can find the equilibrium attitude parameters iteratively. Even with given trim and sinkage, the wetted hull lengths are not known in advance and are a part of the solution. The forward water jet (spray) near the front impingement point on the hull surface is not considered here. As shown below and in previous studies (e.g., Matveev and Ockfen, 2009), the present method works well even with this simplification. Such an assumption is similar to Riabouchinsky closure model commonly employed for developed cavitating flows (Knapp, et al., 1970). A similar schematic was also used in the pioneering works of Butuzov (1966, 1988) on pressurized air cavities under solid surfaces. However, he used fictitious plates near impingement points and applied more computationally expensive continuous source distributions, different from the staggered discrete singularities used here. Some dimensions shown in Fig. 2a are utilized later in Results section.

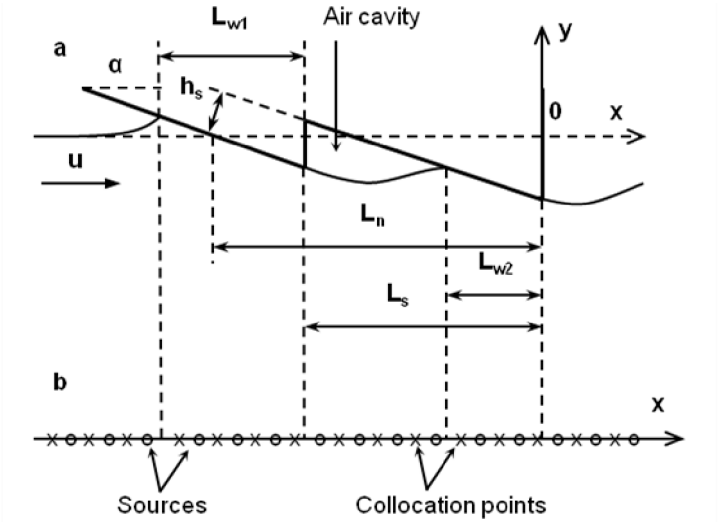

Fig. 2 (a) Schematic of a two-dimensional stepped planing hull with main geometrical parameters. bold lines indicate hull boundaries. (b) Simplistic view of the staggered arrangement of sources (circles) and collocation points (crosses). Distances between singularities are exaggerated. Only a part of the numerical domain is shown.

Under the above assumptions, the Bernoulli equation can be applied on the water boundary streamline,

$$p_0 + \frac{1}{2}\rho u_0^2 = p + \frac{1}{2}\rho u_0^2 + \rho g y \tag{1}$$

where p_0 and u_0 are the upstream pressure and velocity on the free water surface; p, u, and y are the pressure, velo-city, and elevation on the water surface elsewhere; ρ is the water density; and g is the gravity constant. Only a linear problem is considered here that implies small water slopes and hull trim angles. This assumption also restricts hull slopes to small angles. However, most planing hulls, at least when operating in efficient regimes, have small slopes of surfaces in contact with water. Therefore, a linearized form of the Bernoulli equation on the free water surface is appropriate for the present analysis,

$$\frac{\sigma}{2} = \frac{u'}{u_0} + \frac{g\,y}{u_0^2} \tag{2}$$

where $\sigma = (p_0 - p)/(\rho u_0^2/2)$ is named here as the ventilation number (zero on the free surface open to atmosphere and non-zero on the surface of a pressurized cavity between the hulls) and $u' = u - u_0$ is the perturbation velocity. The ventilation number (Eq. 2) is defined similarly to the cavitation number commonly used for characterizing natural cavitation of propellers and high-speed underwater projectiles. In contrast to the cavitation number, the ventilation number can be negative. On the wetted hull surface, the same Eq. (2) holds, but an unknown and space-dependent pressure coefficient with minus sign must be used instead of the ventilation number, i.e., $C_p = (p - p_0)/(\rho u_0^2/2) = -\sigma$.

For solving Eq. (2), hydrodynamic point sources are distributed along the horizontal line with $y = 0$. The staggered scheme is applied for positioning collocation points where Eq. (2) is satisfied (Fig. 2b). Placing them between the sources and one point in front of the most upstream source minimizes the influence of the downstream boundary of the numerical domain (Bertram, 2000). The velocity perturbation in Eq. (2) is then calculated by summing contributions from all sources,

$$u'(x_i^c) = \frac{1}{2\pi}\sum\nolimits_j \frac{q_j}{x_i^c - x_j^s} \tag{3}$$

where x_i^c and x_j^s are positions of the *i*-th collocation point and the *j*-th source with strength q_j. The linearized kinematic boundary condition on the free surface relates the surface slope to the intensity of local sources (Matveev, 2007),

$$\frac{1}{2}\left(\frac{q_i}{\Delta x_i} + \frac{q_{i-1}}{\Delta x_{i-1}}\right) = -2u_0\,\frac{y_i^s - x_{i-1}^s}{x_i^s - x_{i-1}^s} \tag{4}$$

where Δx is the cell size and y^s is the water surface elevation at a source location. On the wetted hull surface, this elevation and the source strength are related to the known hull geometry.

The linear system of equations, involving Eqs. (2-4) and conditions on the hull surface and at the upstream point (undisturbed flow), can be solved to determine the water surface elevations and source intensities. If the number of source/collocation pairs is *N*, there will be 3 *N* equations (Eqs. 2-4 written for each collocation point) and 3 *N* unknowns, including velocity perturbation u'_i, source strength q_i, and either water surface elevation y_i^s (on the free surface) or pressure coefficient C_{pi} (on the hull surface), with index *i* varying from 1 to *N*.

While the water elevation just after hull transom points is known, the positions of the front boundaries of the wetted hull sections have to be found iteratively. Initially, some values of the wetted lengths are guessed. For example, the front points of the wetted surfaces can be selected as intersections of the undisturbed water plane and the hull bottom line. After finding a solution, a water rise in front of the hull is calculated and more accurate estimate for the wetted length is obtained. The calculations are repeated until the elevation of the water at the impinging point becomes equal to the hull vertical coordinate at this location.

With known source intensities and water surface deformations, the pressure distribution on the hull section can be found using Eq. (2) and substituting $-C_p$ instead of σ. Then, the lift coefficient C_L and the center of pressure L_p (with respect to transom) are determined by integrating pressure distribution over the hull surface. The conducted mesh-independence studies suggest that converged results are obtained with the cell size of $L_h/40$ on the hull, where L_h is the overall hull length, and

$\lambda/30$ for zones far from the hull, where $\lambda = 2\pi u_0^2 / g$ is the wavelength on the free water surface. For the entire size of the numerical domain, it is recommended to use one wavelength upstream and 3λ downstream of the hull.

RESULTS

Validation cases

To validate the present mathematical method, numerical results have been compared with a two-dimensional theory for a flat planing plate (Squire, 1957) and experimental data for a model-scale stepped hull with a pressurized air cavity (Matveev, Burnett and Ockfen, 2009). The schematic of the first case, involving a stepless hull, is shown in Fig. 3a. The independent non-dimensional parameter is the Froude number $Fr_{Lw} = u/\sqrt{gL_w}$, based on the wetted length L_w. The first dependent parameter is the linear lift coefficient slope $\partial C_L / \partial\alpha = C_{L1}/\alpha = F_L/(0.5\rho u^2 L_w \alpha)$, where F_L is the lift per unit hull width, and the second parameter is the center of pressure L_p, a distance from transom to the point where the lift force is applied. Results are shown in Fig. 3b,c. The agreement between theoretical results of Squire (1957) and the current method is good. Both models account for gravity. In the limit of $Fr_{Lw} \to \infty$, results of these models approach theoretical values corresponding to a flat plate planing on the weightless liquid: $C_{L1}/\alpha = \pi$ and $L_p / L_w = 3/4$.

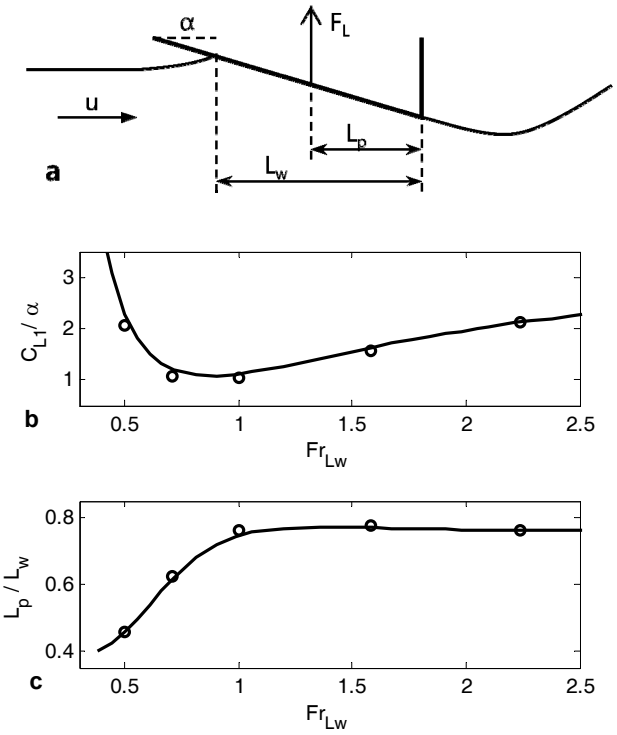

Fig. 3 (a) Schematic of 2D planing plate. (b) Lift coefficient slope. (c) Normalized center of pressure. Circles, theory of Squire (1957); curves, present method.

The second configuration was previously studied experimentally (Matveev, Burnett and Ockfen, 2009). It involves a two-dimensional hull with a step (Fig. 4a). Compressed air was supplied behind the step, and a pressurized air cavity was formed. The maximum (or limiting) length of a stable air cavity depends on the incident flow velocity. The average cavity pressure measured in such limiting regimes was used as an input parameter to the numerical model. Together with the incident flow velocity, it defined the ventilation number in Eq. (2). The experimental and numerical results for the limiting cavity length are presented in Fig. 4b for two step edge submergences. The agreement is reasonably good, indicating that effects of viscosity and surface tension, neglected in the modeling, are relatively unimportant even for this small-scale experimental system. The discussed here validation examples demonstrate the applicability of the current numerical method for planing surfaces, including those with air cavities.

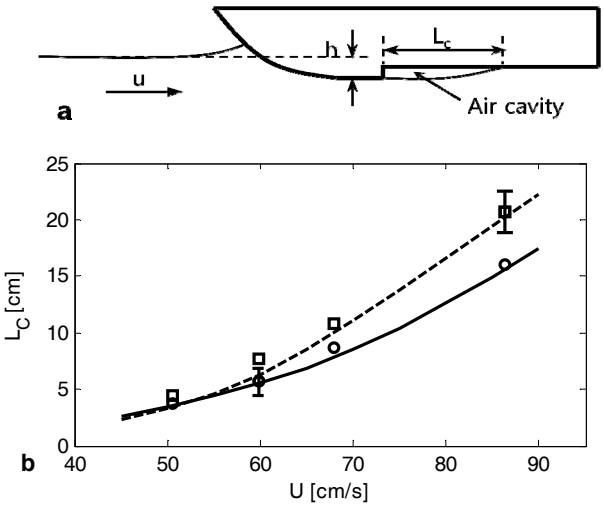

Fig. 4 (a) Schematic of 2D stepped hull with an air cavity. (b) Limiting (maximum) cavity length. Symbols, experimental data (Matveev et al. 2009); curves, present numerical results. Circles and solid curve correspond to step edge submergence h = 1.3 cm; squares and dashed curve to h = 4.1 cm. Vertical bars show total experimental uncertainties.

Single-step hull

In this sub-section, sample calculation results for hydrodynamic characteristics of a stepless hull and stepped hulls with open and pressurized air cavities are presented. The nominal length of both stepless and stepped hulls L_n (Fig. 2a) is kept the same. This length is defined as a horizontal distance from transom to an intersection of the undisturbed water plane and the front hull surface. The Froude number based on this length $Fr_{Ln} = u/\sqrt{gL_n}$ is treated here as a variable parameter. For stepped hulls, the recess length and step height are selected as $L_S = 0.75L_n$ and $h_S = h/6$, where $h = \alpha L_n$ is the nominal transom submergence. Surfaces of the front and rear hulls are flat and parallel. The gage cavity pressure in the case of a pressurized cavity is chosen as a hydrostatic pressure at the level half-way between the step edge and the hull bottom right behind the step. This is done in accordance with previous experimental observations with a two-dimensional air-cavity hull (Matveev, Burnett and Ockfen, 2009).

The output parameters include the lift coefficient slope $\partial C_L/\partial\alpha$ (which equals to C_{L1}/α in the linear problem), normalized center of pressure L_p/L_n, and wetted length L_w/L_n (or two wetted lengths for stepped configurations). In addition, the lift-drag ratio of these hulls is estimated as $LDR = C_L/C_D$, where the lift and drag coefficients are defined as follows,

$$C_L = \frac{F_L}{0.5\rho u^2 L_n} \tag{5}$$

$$C_D = \alpha C_L + C_f \frac{L_w}{L_n} \tag{6}$$

The first term on the right-hand side of Eq. (6) corresponds to the lift-induced drag, while the second term is due to frictional drag. This equation is similar to those commonly used for estimating drag of planing hulls (e.g., Savitsky, 1964). The lift-drag ratio is evaluated below assuming realistic values for the trim angle, α = 0.0698 radian (or 4°), and frictional drag coefficient, C_f = 0.003. In the case of stepped hulls, the wetted length in Eq. (6) is the sum of wetted lengths on both hulls: $L_w = L_{w1} + L_{w2}$.

The calculation results are shown in Fig. 5. The lift coefficient slope and lift-drag ratio initially decrease with increasing Froude number and then increase for $Fr_{Ln} > 1$. This dependence is associated with a dominant hydrostatic support at low speeds and high dynamic lift at high speeds. The stepless hull has higher lift coefficient than stepped hulls (Fig. 5a), while the lift-drag ratio of the stepless hull is inferior to stepped configurations at higher speeds (Fig. 5b), especially to the hull with a

pressurized air cavity. The center of pressure with respect to the nominal length increases with Froude number, due to transition to dynamic support and increase of the wetted length (Fig. 5c). The wetted length of the stepless hull, as well as the wetted lengths of front surfaces on the stepped hulls, increases with speed (Fig. 5d). The wetted lengths of rear hulls decrease, and this reduction is more pronounced for a hull with a pressurized cavity. The reduction of wetted lengths on stepped hulls results in higher lift-drag ratio, as shown in Fig. 5b.

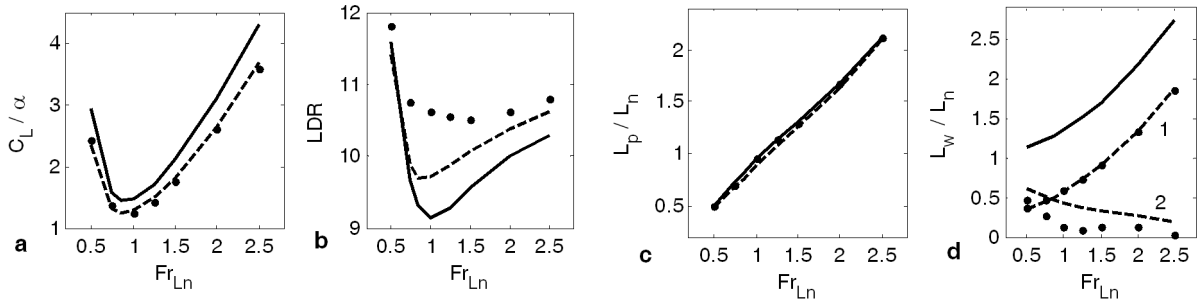

Fig. 5 Comparison of hydrodynamic characteristics of stepless hull (solid line), stepped hull with open cavity (dashed line), and stepped hull with pressurized cavity (circles). (a) Lift coefficient slope, (b) lift-drag ratio, (c) normalized center of pressure, and (d) normalized wetted lengths. In sub-figure (d), labels 1 and 2 correspond to front and rear hulls, respectively (as shown in Fig. 2a).

Distributions of the pressure coefficient on three studied hulls at Fr_{Ln} = 0.75 and 1.5 are illustrated in Fig. 6. The highest pressure values are achieved near leading points of the wetted surfaces. In case of a stepless hull, pressure generally decreases toward the trailing edge. However, at sufficiently low speeds pressure can locally increase toward the transom due to significant hydrostatic lift component of deeper (aftward) hull sections (Fig. 6a). In the case of stepped hulls, there are areas with zero (open cavity) and finite (pressurized cavity) gage pressure corresponding to air cavities. These areas are followed by wetted surfaces of rear hulls with peaks of pressure in the beginning of these sections. The wetted length of the rear hull is significantly shorter in the case of the hull with a pressurized cavity (as also shown in Fig. 5d), which results in lower friction drag.

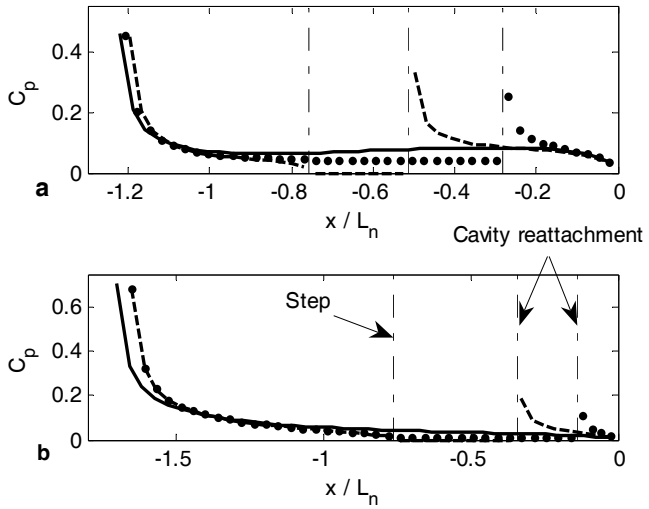

Fig. 6 Examples of pressure coefficient distribution. (a) Fr_{Ln} = 0.75, (b) Fr_{Ln} = 1.5. solid line, stepless hull; dashed line, stepped hull with open cavity; circles, stepped hull with pressurized cavity. Dash-dotted lines indicate locations of the step edge and cavity reattachment points.

Trim tabs are often used on fast planing boats to change its trim angle or to augment lift. The effect of trim tab deployment can be easily modeled by the present numerical method. A schematic of a two-dimensional planing hull with a trim tab is shown in Fig. 7a. Sample calculations have been carried out for stepless and open-cavity stepped hulls at Fr_{Ln} equal to 0.75

and 1.5 and the relative tab length L_t / L_n = 1/8. The variable parameter is a deflection of the tab trailing edge h_t normalized by the nominal hull submergence $h = \alpha L_n$. The calculation results are shown in Fig. 7b,c. The augmentation of lift coefficient is proportional to the tab deflection. The center of pressure moves aftward with the tab deployment, which would result in decreased trim angle on a freely moving boat. Effects of a trim tab deflection are similar for the considered configurations of stepless and open-cavity stepped hulls.

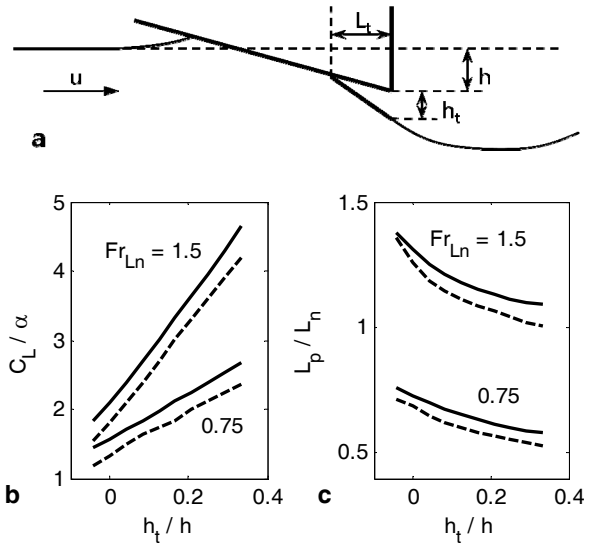

Fig. 7 (a) Schematic of trim tab arrangement on a stepless hull, (b) lift slope coefficient, (c) normalized center of pressure. Solid lines, stepless hull; dashed lines, stepped hull with open cavity.

Multi-step hull

Planing surfaces designed for ultra-fast regimes often involve multiple transverse steps. Such configurations are commonly used on hulls of hydrofoil craft and wing-in-ground effect vehicles that are designed to exit from water at sufficiently high speeds. Within the two-dimensional consideration, planing hulls with multiple steps can be also modeled by the present method. As an example of one multi-step system, an infinite series of identical stepped hulls is considered here (Fig. 8). The flow is periodic in this setup with a spatial period being the distance L between transoms of neighboring hulls.

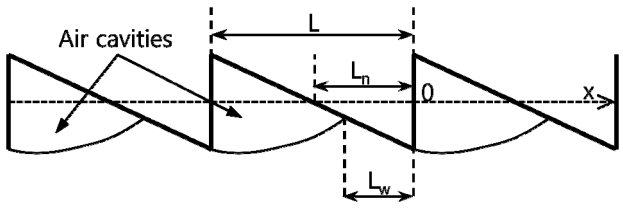

Fig. 8 Portion of infinite periodic series of stepped hulls. Solid surfaces are shown in bold lines. Dotted line corresponds to the undisturbed water surface level.

The hydrodynamic model described above can be applied for this case as well, but the perturbation velocity in Eq. (3) must be changed to account for contributions from an infinite series of sources. Due to a periodic nature of the problem, this velocity can be calculated as follows,

$$u'(x_j^c) = \frac{1}{2\pi} \sum_j \sum_{n=-\infty}^{n=+\infty} \frac{q_j}{x_c^c - x_j^s + nL} \tag{7}$$

where the first sum is taken over sources within one section, e.g., $-L < x < 0$. It can be shown that the infinite series in Eq. (7) converges and results in the expression similar to Eq. (3) with a correction coefficient,

$$u'(x_j^c) = \frac{1}{2\pi}\sum_j \frac{q_j}{x_c^c - x_j^s} I(\beta_{ij}) \tag{8}$$

$$I = \frac{\pi}{\beta}\frac{\sin(2\pi/\beta)}{1-\cos(2\pi/\beta)} \tag{9}$$

$$\beta_{ij} = \frac{L}{x_i^c - x_j^s} \tag{10}$$

Parametric calculations have been conducted for cases with $Fr_{Ln} = 0.75$ and 1.5 and $\sigma = 0$ (open cavities). The normalized spacing between hulls L/L_n is treated as a variable parameter. Results for the lift coefficient slope, lift-drag ratio (trim angle and friction coefficient are the same as in the single-step example), center of pressure, and wetted length are shown in Fig. 9. These results show periodic solutions with respect to L/L_n, which are associated with the wave pattern between hulls (Fig. 10). This period is longer for higher Fr_{Ln} (Fig. 9) because of longer wavelength on the water surface. Due to limited horizontal scale in Fig. 9, oscillations of results at $Fr_{Ln} = 1.5$ are not clearly visible.

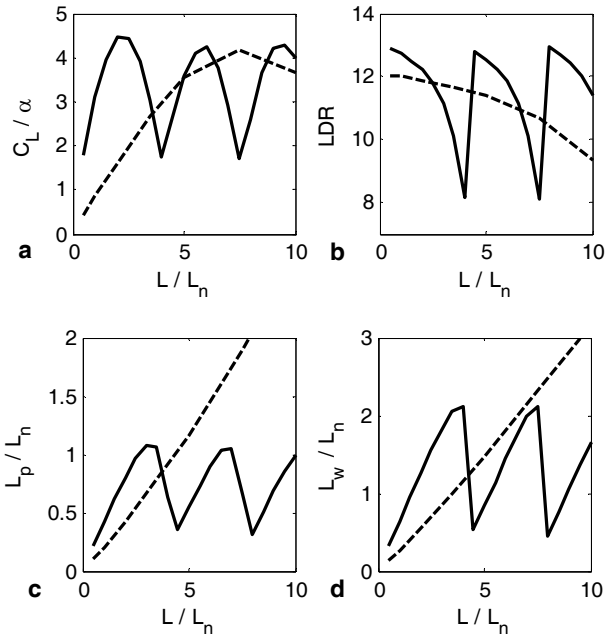

Fig. 9 Hydrodynamic characteristics of one planing surface in the infinite series of hulls. Solid lines, $Fr_{Ln} = 0.75$; dashed lines, $Fr_{Ln} = 1.5$. (a) Lift coefficient slope, (b) lift-drag ratio, (c) normalized center of pressure, and (d) normalized wetted length.

At sufficiently low L/L_n, the water contour resembles a fraction of the wave on the free surface (Fig. 10a). With a gradual increase of the hull spacing, the wetted length L_w/L_n also increases (Fig. 9d). However, at some value of the hull spacing, the crest of the first wave behind transom is unable to reach the hull surface. The water impingement point then jumps to a downstream location where the second water rise is present and the hull surface is deeper (Fig. 10b). Therefore, variations of hydrodynamic characteristics are repeated with further increasing L/L_n (Fig. 9), since they are sensitive to the pattern of water flow impinging on the hull surface. The next jump occurs with when the second wave crest becomes lower than the hull surface

at its location, and another jump of the impingement point happens (Fig. 10c). These results indicate a strong sensitivity of hydrodynamic properties to the hull spacing and Froude number. The present method can be used to estimate these effects in the preliminary design stage.

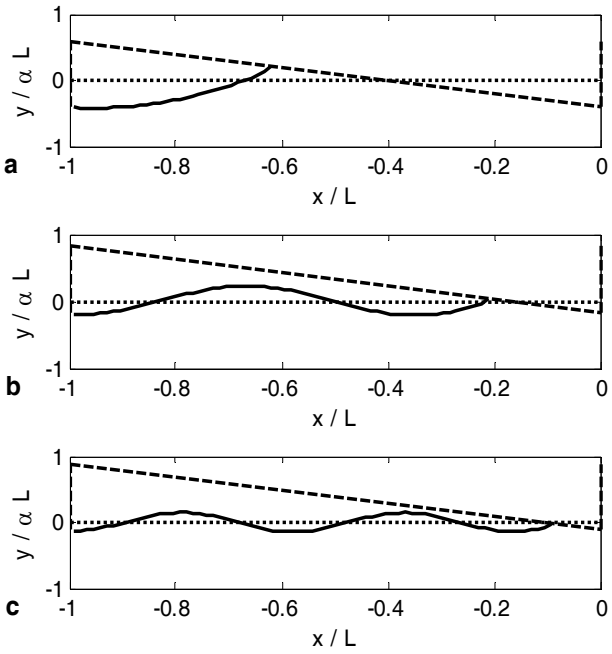

Fig. 10 Water surface elevations (solid lines) between planing hulls in the infinite series at $Fr_{Ln} = 0.75$. Hull surface is shown by dash lines. Undisturbed water surface level is indicated by dotted line. (a) $L / L_n = 2.5$, (b) $L / L_n = 5.5$, (a) $L / L_n = 8.5$.

CONCLUSIONS

A method of hydrodynamic point sources has been successfully applied for modeling stepped planing hulls in the two-dimensional formulation. This method is found to produce results in a good agreement with an available theory for a planing flat plate and experimental data for a pressurized air cavity under a surface hull. Parametric calculations with a single-step two-hull setup demonstrated non-monotonic dependence on Froude number and suggested that a stepped configuration can be more efficient than a stepless hull, although it generates lower lift at the same hull position. A pressurized air cavity further reduces the wetted length on the rear hull, resulting in even higher lift-drag ratio. The present method can be used to analyze more complex hull geometries, for example, with a bottom camber or trim tabs. The effect of a trim tab deflection has been presented for selected configurations. The conducted analysis of an infinite series of stepped planing surfaces is relevant to multi-step setups used on ultra-fast hulls. A periodic dependence of hydrodynamic characteristics on the relative hull spacing is observed, associated with the wave pattern between neighboring hulls.

The main advantage of the present numerical method over added-mass strip theories is an explicit computation of the water surface around planing hulls, which is critically important for calculation of interacting multi-hull systems. In comparison with complete viscous modeling by finite-volume methods, the present model is much less computationally expensive, which makes it suitable and efficient for initial parametric design calculations. Future extensions of the current work can address three-dimensional hulls and nonlinear flow effects. Simulation of unsteady regimes would require modification of governing equations to account for time-dependent flow properties.

ACKNOWLEDGEMENT

This material is based upon work supported by the National Science Foundation under Grant No. CMMI-1026264.

REFERENCES

Benedict, K., Kornev, N., Meyer, M. and Ebert, J., 2002. Complex mathematical model of the WIG motion including the take-off mode. *Ocean Engineering*, 29(3), pp.315-357.

Bertram, V., 2000. *Practical Ship Hydrodynamics*. Oxford : Butterworth-Heinemann.

Butuzov, A.A., 1966. Limiting parameters of an artificial cavity formed on the lower surface of a horizontal wall. *Fluid Dynamics*, 1(2), pp.167-170.

Butuzov, A.A., 1988. Spatial linearized problems on flow around ship bottom with artificial cavitation. Shipbuilding Problems, *Ship Design Series 8*, pp.1-18.

Caponetto, M., 2001. Practical CFD simulations for planing hulls. *Proceedings of the 2nd International Conference on High-Performance Marine Vehicles*. Hamburg.

Doctors, L.J., 1974. Representation of planing surfaces by finite pressure elements. *Proceedings of the 5th Australian Conference on Hydraulics and Fluid Mechanics.* Christchurch, New Zealand.

Faltinsen, O.M., 2005. *Hydrodynamics of High-Speed Marine Vehicles*. New York : Cambridge University Press.

Knapp, R.T., Daily, J.W. and Hammit, F.G., 1970. *Cavitation*. New York : McGraw-Hill.

Lai, C. and Troesch, A.W., 1996. A vortex lattice method for high-speed planing. *International Journal for Numerical Methods in Fluids*, 22(6), pp.495-513.

Martin, M., 1978. Theoretical determination of porpoising instability of high-speed planing boats. *Journal of Ship Research*, 22, pp.32-53.

Matveev, K.I., 2005. Application of artificial cavitation for reducing ship drag. *Oceanic Engineering International*, 9(1), pp.35-41.

Matveev, K.I., 2007. Three-dimensional wave patterns in long air cavities on a horizontal plane. *Ocean Engineering*, 34(13), pp.1882-1891.

Matveev, K.I. and Ockfen, A., 2009. Modeling of hard-chine hulls in transitional and early planing regimes by hydrodynamic point sources. *International Shipbuilding Progress*, 56(1-2), pp.1-13.

Matveev, K.I., Burnett, T. and Ockfen, A., 2009. Study of air-ventilated cavity under model hull on water surface. *Ocean Engineering*, 36(12-13), pp.930-940.

Payne, P.R., 1988. *Design of High-Speed Boats: Planing*. Fishergate, Annapolis, MD.

Savitsky, D., 1964. Hydrodynamic design of planing hulls. *Marine Technology*, 1(1), pp.71-96.

Squire, H.B., 1957. The motion of a simple wedge along the water surface. *Proceedings of the Royal Society*. 243(1232), pp.48-64.